DEUTSCHES ELEKTRONEN-SYNCHROTRON DESY

DESY SR-71/4
August 1971

A Grazing Incidence Vacuum Ultra-Violet Monochromator with Fixed Exit Slit

by

H. Dietrich and C. Kunz

2 HAMBURG 52 · NOTKESTIEG 1

To be sure that your preprints
are promptly included in the
HIGH ENERGY PHYSICS INDEX, send
them to the following address
(if possible by air mail):

A Grazing Incidence Vacuum Ultra-Violet Monochromator with Fixed Exit Slit

H. Dietrich and C. Kunz

Deutsches Elektronen-Synchrotron DESY, Hamburg, Germany

A new monochromator with parallel incident light, a fixed exit aperture and higher order rejection properties has been built and tested with the 7.5 GeV electron accelerator DESY which was used as a synchrotron light source. The parameters of the instrument are chosen to match the source characteristics at DESY. The exit beam is focused on a spot of 50 µm x 300 µm at the exit slit yielding about 10^7 monochromatic photons/sec at the intensity maximum (100 Å). The resolution attained is about 500 over the whole range 40 - 350 Å. Virtually no higher order admixing occurs in this range. The instrument can be used up to 1000 Å in a different mode of operation with less ideal performance.

I. INTRODUCTION

Two years ago we published the principle of a new monochromator mounting[1] which promised to overcome several of the deficiencies of grazing incidence vacuum ultraviolet monochromatization[2]. At that time construction of such an instrument with parameters chosen to match the geometry at the DESY electron synchrotron[3] was begun. In the meantime this instrument has been completed and thouroughly tested.

The most common spectrograph mounting in the wavelength range below 400 Å is the grazing incidence Rowland mounting[2]. Two major disadvantages of this mounting are the overlapping of higher orders and the continuous change of the exit (or entrance) path when the instrument is operated as a monochromator. Severe limitations arise when immovable light sources are used at the entrance arm and sensitive or heavy components are attached to the exit arm (e.g. a UHV reflectometer). In any of the classical Rowland mountings either the source or the detector plus experimental arrangements have to be moved when scanning the spectrum. Only recently have Codling and Mitchell[4] overcome this problem by designing a Rowland spectrograph with rotating mirrors at the entrance and exit slits and a grating scanning along the Rowland circle. We shall later compare this instrument with ours in detail.

The operation principle of our monochromator is illustrated in Fig. 1. First consider a fixed wavelength λ in Fig. 1 (a). Parallel light is incident from the left, on the mirror M, with a grazing angle ϕ_M, and is reflected to the plane grating G. The grazing angle ϕ_G of the light incident on the grating is equal to ϕ_M so that the λ=0 direction is parallel

to the primary direction. Only light emerging from the grating in a definite fixed direction given by the angle γ(and thus of a certain wavelength λ) is accepted by the angle-defining system which consists of a fixed spherical or paraboloid focusing mirror F and the exit slit S.

Change of wavelength is illustrated in Fig. 1 (b) and (c). The mirror M moves along the linear path $\overline{AB}$ and at the same time turns about an axis α_M in such a way that it always illuminates the grating. Simultaneously, the grating G turns about the axis α_G so that it is always parallel to the mirror M. The angles $\Phi_M=\Phi_G$ increase continuously and at the same time the wavelength λ passing through the exit slit increases.

The main properties of this mounting are:

(1) The exit direction and exit slit are fixed.

(2) The blaze angle of the grating can be chosen to be half the angle γ so that the grating will operate for all wavelengths in the blaze maximum

(3) Use is made of the fact that there is a minimum wavelength reflected by a surface, depending on the angle of incidence on the surface. The parameters of the monochromator can be chosen to suppress higher-order reflections from the grating over a wide range.

(4) The energy resolution for a fixed exit slit is nearly proportional to the photon energy which results in constant resolving power.

The use of such a spectrograph is not limited to synchrotron radiation sources. Any distant source like astronomical objects in space physics could be analyzed with an instrument of this type. With another concave mirror in front of the present pre-mirror this mounting could also be converted into a monochromator with an incorporated entrance slit.

We shall give a detailed discussion of the parameters of the instrument in Section 2. Section 3 contains a description of the mechanical set-up while Section 4 is concerned with the alignment and calibration of the monochromator. Tests and spectra obtained with synchrotron radiation are discussed in Section 5. Finally in Section 6 we compare this instrument with others available for this spectral range.

II. THE PARAMETERS OF THE DESY MONOCHROMATOR

Properties of the synchrotron source

In order to understand the performance of the monochromator better a short description of the properties of synchrotron radiation at DESY is given[3]. The source is the electron beam in one bending magnet (radius 31.7 m)of the accelerator. The beam dimensions depend on the maximum energy of the accelerator and its mode of operation, typical values being 10 mm in the horizontal (radial) and 2 mm in the vertical direction.

Radiation is emitted in the instantaneous direction of flight of the electrons with a small angular width. For 6 GeV maximum energy and 100 Å wavelength the light beam has a vertical extension of ∿5 cm at a distance of 40 m at the experimental area. The horizontal extension is only given by the width of the vacuum pipe guiding the beam since electrons radiate in a magnet at any point of their curved path.

The spectrum is continuous in wavelength and extends from the visible down to the X-ray range. The radiation is highly polarized; polarization is 100 % for radiation emitted directly in the plane of the synchrotron with the electrical vector lying horizontally. Typically about 10^{11} photons are emitted at about 100 Å wavelength into a 1 Å interval per cm^2 beam cross section at the experimental site.

Dispersion, resolving power

In order to avoid the low reflectivities for p polarized light the mirror M and the grating G in Fig. 1 have to be arranged in such a way that the light is reflected and dispersed on a vertical plane. These reflections should increase the high degree of polarization of the synchrotron light to almost 100 %.

The wavelength λ as a function of Φ_G is given by

$$\lambda = D\ (\cos\Phi_G - \cos(\Phi_G + \gamma)) \tag{1}$$

$$\sim D\gamma(\sin\Phi_G + \frac{1}{2}\ \gamma\cos\Phi_G)$$

where D is the grating constant. The parameters Φ_G and γ are explained in Fig. 1. The wavelength resolution $\Delta\lambda$ is given by:

$$\Delta\lambda \simeq (\frac{\lambda}{\gamma} + \frac{1}{2}\ D\gamma\ \cos\Phi_G) \tag{2}$$

with $\Delta\Phi$ being the angular resolution.

In actual cases the second term on the right side is negligible for all but the shortest wavelengths. If we neglect this term and substitute ΔE the energy resolution, a quantity, which is of more interest than $\Delta\lambda$ for solid state physics, we obtain:

$$\frac{\Delta E}{E} \simeq \frac{\Delta\Phi}{\gamma} \tag{3}$$

where E is the photon energy. As an example we take $\Delta\Phi=5\cdot10^{-5}$ rad, $\gamma=0.05$ rad, E=100 eV and obtain $\Delta E=0.1$ eV. This gives a resolving power $\Delta E/E=1:1000$.

Suppression of higher orders

The minimum wavelength λc reflected by a grating or a mirror is given in rough approximation by

$$\lambda c = \Lambda_o \sin(\Phi_G+\beta) \approx \Lambda_o(\sin\Phi_G+\beta\cos\Phi_G) \qquad (4)$$

where $\beta(=\gamma/2$ in our case) is the blaze angle of the grating. Λ_o is a constant for which we took the value $\Lambda_o \approx 300$ Å. This value was obtained from the experiences with a Rowland monochromator[5] operated with gold coated gratings under different angles of incidence. Higher order contamination of the light at wavelength λ is absent if the relation

$$\lambda/2 < \lambda_c < \lambda \qquad (5)$$

holds. In actual cases this cutoff λ_c is not sharp as exemplified for Pt in Fig. 2. The optical constants on which these calculations are based were taken from Roemer[6].

By comparing Eq. (1) to Eq. (4) it becomes clear that a good choice of the parameters is achieved when $D\gamma \approx 1.5\ \Lambda_o \approx 450$ Å. Then suppression of the higher orders should result. We chose the minimum wavelength of the instrument to be 40 Å in order to cover the range down to the carbon K edge at 44 Å. Then through Eq. (4) the minimum grazing angle of incidence is $\Phi_G \sim 4^o$. This fixes the ratio $a:\overline{AB}$ (Fig. 1). We chose $\overline{AB} = 240$ mm and $a = 30$ mm. Since $\gamma = 2\beta$ influences the cutoff of the grating (Eq. 4), γ has to be smaller than 4^o. On the other hand γ should not be too small because stray light becomes stronger in the vicinity of the λ=0 direction. Especially the focusing mirror F should not be hit by the direct image. So

chose a plane grating (Bausch and Lomb) with 1200 lines/mm and a blaze of 1.5° (γ=3°). The grazing angle of incidence to the focusing mirror F was fixed at 0.1 rad (≈5.7°). With these parameters the monochromator covers the range 40 to 350 Å. At 350 Å Φ_G is 50°.

If only the grating be rotated wavelengths above 350 Å can be scanned. The mechanism was planned in such a way that the coupled motion could be stopped at any position and the grating could scan alone. At $\Phi_M = 45°$ Φ_G needs only to change by ≈3 degrees in order to cover the wavelength range up to 1000 Å.

Double grating Monochromator

Another version of the monochromator results when the mirror M in Fig. 1 is replaced by another grating. Fig. 3 shows the principle of this mounting. The two gratings G_1 and G_2 must be identical and have to be irradiated with the same entrance angle. The wavelength selected emerges parallel to the entrance direction. Therefore the angle defining system has to be rearranged. When a focal mirror F with altered focal length is installed at point P_2 (instead of point P_1) the exit slit and exit direction can be the same as before. Equation (1) is again valid but the wavelength range covered is slightly changed. The right hand side of Eq. (2) has to be multiplied by

$$\frac{1}{1 + \frac{\sin\Phi_G}{\sin(\Phi_G+\gamma)}}$$

which gives an improvement in resolution by a factor of approximately 1/2 for angles of incidence Φ_G which are not too small. The main advantage is the lower background of straylight in this mode of operation. Up to now we have not tried this version.

Optical elements

Table 1 gives a survey on the properties of the optical components. We tried both a spherical and a paraboloid focusing mirror. The spherical mirror had a radius R=20 m. In this case a line focus of about 20 mm length is obtained. The imaging error causes a width σ of the focus of

$$\sigma = \frac{3}{2}\,\frac{w^2}{R} \tag{7}$$

where 2w is the illuminated length of the mirror. In case of a 7 mm high bundle we get σ = 100 µm which by itself would restrict the angular resolution to $\Delta\Phi = 10^{-4}$ rad.

We were able to obtain a high quality paraboloid mirror with the parameters given in Table 1. This mirror was ground from glass and tested interferometrically by the manufacturer. It gives a stigmatic image of the source and almost permits obtainment of the theoretical resolution even with a wide bundle under favourable circumstances.

Since the distance of the source from the monochromator is g_o = 40 meters and since the grating can then not be considered to act as a simple mirror the image formed by the paraboloid mirror F is situated not at the distance f for parallel light (f = 1 meter) but at f + Δf with

$$\Delta f = \frac{f^2}{g_o} \cdot \frac{\sin^2\Phi_G}{\sin^2(\Phi_G+\gamma)} \tag{8}$$

The vertical size of the image is

$$v = v_o\,\frac{f}{g_o} \cdot \frac{\sin\Phi_G}{\sin(\Phi_G+\gamma)} \tag{9}$$

while the horizontal width, which has no influence on the resolution, is $l = l_o \cdot f/g_o \approx 250$ m with v_o and l_o being the vertical and horizontal sizes of the beam in the synchrotron and v and l the equivalent sizes of the image. The sine factor can easily be derived with the help of the grating equation. (In the case of the double grating monochromator the sine factors have to be squared.) Δf varies between 0.8 cm and 2.5 cm, v between 30 µm and 50 µm (for $v_o \approx 2$ mm). We have therefore supported the exit slit on a sled which allows for the adjustment of its distance from the mirror F by ~ 30 mm for optimum performance.

III. MECHANICAL DETAILS

General layout

Figure 4 is a schematic diagram of the complete instrument including vacuum chamber and supports. The monochromator itself consists of two separate vacuum housings, one holds the mirrors and the grating (unit I) and the other the exit slit assembly (unit II). Since any motion or vibration of these units is adverse they are decoupled from the vacuum housing by soft bellows (B) and the supports are tightly screwed to the floor. An isolated separate foundation would have been preferable since it turned out that the vibrations transmitted by our laboratory floor are still of considerable influence.

Unit I is kinematically supported. All the motors driving the adjustable and scanning parts are incorporated into this unit. The whole unit can, therefore, be lifted out and put back reproducibly in an easy fashion. The top part of the vacuum recipient can be hydraulically lifted permitting easy access from all sides. The pumping system consists of one 250 l/s turbo-mulecular pump (TMP) and two 230 l/s ion-getter pumps GP. The end vacuum which was obtained routinely is $2 \cdot 10^{-7}$ torr.

Two adjustable apertures A_1 and A_2 limit the size of the beam (horizontally 20 mm, vertically 0-10 mm). They are monitored, like most of the adjustable parts by potentiometers and adjusted under operational conditions by small ungreased epoxy insulated motors (Mauthe). Figure 5 is a photograph of the instrument with the cover of the large vacuum tank lifted and unit I exposed.

The angular coupling mechanism

The coupling mechanism by which the motion of mirror M and grating G outlined in Fig. 1 is achieved determines the quality of the instrument. The principle of this mechanism is shown in Fig. 6. The direction of the beam reflected by mirror M onto the center of the grating G is substantiated by the arm GS which is rotating around the grating axis αG and rolling on a bearing which is sitting on the pre-mirror axis αM. Two rhombusses serve to divide its angular motion by two. The arm b of the pre-mirror rhombus and the arm c of the grating rhombus are always parallel to GS. If the arms a and d are kept in fixed directions the sliding diagonals rotate pre-mirror and grating as desired. Arm a can be adjusted slightly to bring the mirror into the correct initial position. All arms of the rhombusses are specified to be equal in length (100 mm) to within a few microns. The joints are equipped with paired high precision ball-bearings to eliminate play (RMB). The sliding surfaces of parts GS, f and e are lapped with an accuracy of 1 - 2 μm. As almost all parts of the whole instrument these parts are made of stainless steel.

For the second type (uncoupled) scanning mode the coupled motion is stopped at any position, then arm d is rotated by a potentiometer controlled precision screw. The position where the grating is parallel to the pre-mirror can again be precisely restored and the coupled motion can continue.

Drive mechanism, special features

Figure 7 shows a more detailed diagram of the spectrograph. The sled (SL) which holds the pre-mirror M moves along two stainless steel rods (R) (30 mm thick, 380 mm long), which are ground with an accuracy of 2 μm. The sled slides on teflon pieces which are capsuled in metal to avoid flowing and

thus continuous misalignment. Teflon was superior to several other bearing materials which we tried. The sled and, secondarily, the whole coupled motion is driven by a precision screw AS (Transrol) which has a nut holding planet screws. The nut is divided for adjusting the back lash. The linearity error of this screw is smaller than 10 ,m. The screw is coupled to a 40 turns precision potentiometer P1 (Litton). This, together with the screw, is driven by a speed regulated motor 10 - 3000 rpm (Motomatic) resulting in scanning at a speed of 0.03 - 1 eV/sec. Potentiometer, motor (MT) and gear (GT) are capsuled together in a container which holds atmospheric pressure.

IV. ALIGNMENT PROCEDURE AND CALIBRATION

The alignment has three steps. First the axis of rotation of the pre-mirror is aligned parallel to the axis of rotation of the grating. Then the direction of synchrotron light is simulated by a laser beam to align pre-mirror and grating in the beam and pre-align the focusing mirror and exit slit. Finally, with synchrotron light, the parabolic focusing mirror and the position of the exit slit are adjusted for optimum resolution.

Pre-mirror and grating

The alignmeht of pre-mirror and grating is achieved by using an auto-collimating telescope and an auxiliary vertical plane mirror behind the grating which serves to reflect the light beam back into itself. At the same time the auto-collimating telescope permits looking past the pre-mirror and the grating directly into this mirror. The horizontal displacement of these two images at different positions of the scanning drive serves to adjust the pre-mirror axis parallel to the grating axis with the help of the adjustable teflon bearings of the sled.

The vertical displacement of the two images serves to make Φ_G and Φ_M of Fig. 1 equal. With the auto-collimating telescope this adjustment was checked over the whole range of the coupled scanning motion with a sensitivity of 10^{-5} rad. The resulting measured deviation $(\Phi_G - \Phi_M)$ is plotted in Fig. 8. It turns out that this deviation is much larger than expected from the mechanical tolerances given to the manufacturers of the parts which determine the angular division. Yet this curve was found to be reproducible within $2 \cdot 10^{-5}$ over a period of 1/2 year when scanning in the same direction. It is not clear from such a curve which part of the coupling mechanism introduces the main error.

Nevertheless it can be shown that this curve allows, with a sufficient accuracy, for the correction of the wavelength derived from an idealized motion of the scanning mechanism.

Focusing Mirror

All the alignments with the laser beam replacing the synchrotron light are straight forward. After that the most tedious part of the whole alignment is the optimization of the paraboloid mirror and exit slit. First the grating is rotated out of the parallel position by an angle $\gamma/2$ until the zero order light passes through the exit slit. Using wide bundless an exit slit of only 10 µm and a reduction of the source size to ≈0.5 mm by a special slit in the beam pipe near the synchrotron maximum sensitivity to defocusing is achieved. The angle of incidence onto the paraboloid mirror, the rotation around the surface normal of this mirror and the position of the exit slit are adjusted for optimum width of the direct image. This width is measured by rotating the grating. It turned out that vibrations in the laboratory were a serious problem. All the turbo-mulecular pumps had to be turned off and the vacuum was only maintained by ion getter pumps for obtaining an optimum width of the direct image. The smallest width achieved in this way was 30 µm.

Calibration

The wavelength is determined through equation 1 with

$$\Phi_G = 45^o - 1/2 \ \text{arctg} \left(\frac{x_{45} - x}{a}\right) \qquad (10)$$

together with the corrections shown in Fig. 8. The parameter a is indicated in Fig. 1 and x is the position co-ordinate of the sled measured along $\overline{AB}$

while x_{45} is the value of this co-ordinate when $\Phi_G = 45^o$. The three parameters which have to be determined are γ, a and x_{45}.

The following positions of edges or lines served to calibrate these parameters: Ar 50.72 Å, Kr 135.88 Å ± 0.10, Xe 190.41 Å ± 0.10, Ne 272.10 Å ± 0.05 Å, Al 170.49 ± 0.05 Å, (Mg 250.02, NaCl 61.42).

The optimum values for the three unknown parameters were calculated by an iterating computer program which minimizes the mean square deviations. For good values of these parameters a minimum of five well distributed calibration points are necessary.

V. PERFORMANCE

Intensity, suppression of higher orders, stray light

Figure 9 shows the spectrum obtained with an open photomultiplier (Bendix 306) when the light hits the W-cathode at a grazing angle of $\sim 20^{\circ}$ (solid line). From the statistical fluctuations the number of pulses at the maximum at $\sim$100 Å was estimated to be $\sim 10^{6}$. This has to be multiplied by the unknown efficiency of the W-cathode in order to obtain the number of photons/sec through a 40 µm slit. The number of photons which would pass the monochromator in case it had 100 % transparency is given in Table 2.

The steep decrease in reflectivity below 100 Å seems to be explainable by the reduction of reflectivity of the uncoated paraboloidal mirror in this range. Also the reduction of the size of the bundle comes into play. At 44 Å a dip is observed which was growing with time, obviously because of growing carbon contaminations on the reflecting surfaces. The reduction of intensity for wavelengths above 100 Å is certainly due to the lower reflectivities as exemplified by Fig. 2 for Pt. Other coating materials might yield some improvement in this range.

A good way exists to check whether the parameters (γ and grating constant D) were chosen properly when this spectrograph was designed. The grating could be rotated alone at any position of the pre-mirror thus yielding the dashed curves in Fig. 9. These curves in their low wavelength range resemble quite well the theoretical reflectivity curves of Fig. 2. In order to scan the wavelengths this way it was only necessary to rotate the grating by $\sim 1.5^{\circ}$. Therefore, these curves of Fig. 9 should be comparable to those of Fig. 2. They are, however,

modified by the blaze of the grating. These curves indicate that the higher order radiation should be effectively suppressed; the amount of stray light can be estimated from the low wavelength tail of these curves. Tests with materials showing sharp structures did not show the slightest indication of higher orders.

Non-parallel mode

We also tried another way of operating the system by first rotating the grating by .57° away from the parallel position and then continuing with the coupled motion and a new γ=4.14°. The spectral range covered is then 60-470 Å. Since we have a smaller grazing angle than before for a given wavelength the reflectivity above 200 Å is now considerably increased. Though suppression of higher orders might no longer be perfect over the whole range, tests with NaCl did not show the second order of 60 Å at the 120 Å position and likewise a test with Al did not show the second order of 170 Å at the 340 Å position. The structures of NaCl at ~400 Å indicate a stray light background of several percent which is higher than at shorter wavelengths. This and other possible modifications have to be investigated in more detail in the future.

Resolution

The resolution in the γ=3° mode was tested, not only through the width of the direct image as mentioned in Section 4, but also using sharp structures in the spectra of gases and solids as exemplified in Table 3. These values are lower limits to the resolution since part of the width will be due to the physical nature of these structures. At the beginning of the tests a

spherical focusing mirror was used which, with proper reduction of the bundle cross section, yielded comparable results.

Finally we show an original spectrum of NaCl in Fig. 10 at the onset of $Cl^{-}L_{II,III}$ absorption. This spectrum is in good agreement with measurements of Sagawa et al.[7]. Also part of recently published Argon spectra[8] were obtained using this spectrograph.

VI. COMPARISON WITH OTHER INSTRUMENTS

Miyake et al.[9] have published the design considerations for a similar but much simpler instrument which corresponds roughly to our instrument with the pre-mirror at two different fixed positions and the grating scanning alone. They hope to become free of higher orders in the range 50 - 100 Å and 100 to 200 Å by proper choice of these two positions. We feel that both our calculations shown in Fig. 2 and our curves shown in Fig. 9 demonstrate that this hope for a sharp cutoff wavelength is too optimistic.

When comparing our instrument with the Rowland type monochromator built by Codling et al.[4] we would like to mention the following points:

Both instruments have fixed entrance and exit directions. Their instrument does not reduce higher order contributions, on the contrary the variation of the angle of incidence onto the grating rather enhances the higher orders. Further advantages of our instrument are an almost point-like focus (300 µm x 50 µm) and operation in the blaze maximum. On the other hand the Rowland instrument is capable of operating with different gratings and can achieve a higher resolution in the long wavelength range. This is the main advantage of any Rowland mounting over our mounting. We believe, though, that the resolution, which we are able to obtain is sufficient for most solid state problems.

ACKNOWLEDGMENT

We would like to thank all those persons in the synchrotron radiation group, who have helped this project in various ways either in discussion or through active support. Moreover we would like to thank the workshops of DESY and the II. Institut für Experimentalphysik for skillful handling of tedious mechanical problems.

Literature

1. C. Kunz, R. Haensel, and B. Sonntag, J.Opt.Soc.Am. 58, 1415 (1968)
2. J.A.R. Samson, Techniques of Vacuum Ultraviolet Spectroscopy (J. Wiley & Sons, Inc., New York, London, Sidney 1967)
3. R. Haensel and C. Kunz, Z.Angew.Phys. 23, 276 (1967); R.P. Godwin, Springer Tracts in Modern Physics, Vol. 51 (1969)
4. K. Codling and P. Mitchell, J. Physics E: Sc. Instrum. 3, 685 (1970)
5. R. Haensel, G. Keitel, C. Kunz, P. Schreiber, and B. Sonntag unpublished
6. J. Römer, Diplomarbeit Hamburg 1970
7. T. Sagawa, Y. Iguchi, M. Sasanuma, T. Nasu, S. Yamaguchi, S. Fujiwara, M. Nakamura, A. Ejiri, T. Masuoka, T. Sasaki and T. Oshio, J.Phys. Soc. Japan, 21, 2587 (1966)
8. R. Haensel, G. Keitel, N. Kosuch, U. Nielsen and P. Schreiber, DESY Report 70/47, Sept. 1970
9. K.P. Miyake, R. Kato and H.Yamashita, Science of Light 18, 39 (1969)

Table I: Specifications of the optical components

	description	optical size (mm)	surface accuracy	roughness	surface	manufacturer
pre-mirror	flat	30x30	$\lambda/10$-$\lambda/30$	$\leq$ 30 Å	platinum	Halle Leitz Zeiss
grating	1200 lines/mm flat 1.5° blaze	30x30			gold	Bausch & Lomb
focusing mirror	sphere R=20 m	100x20	$\lambda/20$-$\lambda/30$	10-20 Å	gold	Halle
	paraboloid f=1 m grazing angle 5.7°	100x20	wavefront error $\leq \lambda/8$		glass	Opt... Sur... Ltd.

Table 2: Number of photons which would be available at a 40 Å exit slit under the assumption of 100% transmissivity of the spectrograph. The parameters were: 7.3 GeV energy and 10 mA current in the synchrotron and the effect of a rotating shutter which cuts out every second pulse of the synchrotron.

λ (Å)	Plot/sec
40	$6.65 \cdot 10^9$
70	$4.5 \cdot 10^9$
100	$3.5 \cdot 10^9$
150	$2.67 \cdot 10^9$
200	$2.2 \cdot 10^9$
300	$1.67 \cdot 10^9$

Table 3: Tests of the resolving power

material	λ(Å)	width	$\lambda/\Delta\lambda$
Ar	50.72	0.12	410
NaCl	61.42	0.18	340
Al	170.49	0.44	390
Xe	185.47	0.61	300

Figure Capitons

Fig. 1 Principle of operation of the monochromator. Plane pre-mirror M, plane grating G and focusing mirror F in three stages (a), (b) and (c) of the coupled motion. Parallel, polychromatic synchrotron radiation is incident from the left, monochromatic radiation is emerging from the exit slit.

Fig. 2 Reflectivity R_s for s-polarized radiation of a Pt covered mirror for different grazing angles of incidence ϕ_G calculated from optical constants according to Ref. 6.

Fig. 3 Two grating version of the monochromator. Mirror M in Fig. 1 is replaced here by a grating G_1. Instead of having the focusing mirror at point P_1 one could place an appropriate one now at point P_2.

Fig. 4 Semi-schematic layout of the monochromator. Units I and II are vibrationally isolated from the vacuum housing. They sit on separate supports and are decoupled by soft bellows B. A_1,A_2 = beam apertures, M = pre-mirror, G = grating, S = exit slit, Fi = thin film filters, MP = open photomultiplier, GP and TMP = pumping system.

Fig. 5 Photography of the instrument with unit I exposed. A laser L to the left simulates the incoming synchrotron radiation. Pre-mirror M, grating G and the support of the focusing mirror F can be recognized.

Fig. 6 The coupling mechanism consisting of two angular divides: "pre-mirror rhombus" and "grating rhombus" and the linking arm GS.

Fig. 7 Unit I in detail with the driving mechanism for the coupled motion: a high precision screw AS and the sealed motor MT and potentiometer P_1. The alternative motion, a rotation of the grating only, is driven by the motor GM and monitored by P_2.

Fig. 8 Measured error curve used to correct for the imperfections of the coupling mechanism.

Fig. 9 Measured spectrum without any filters. Full line: coupled mode, broken lines: obtained by stopping the coupled mode at the encircled positions and scanning by rotation of only the grating.

Fig. 10 Transmisivity of an evaporated film of NaCl at the $L_{II,III}$ edges of Cl^-. Compare with Ref. 7.

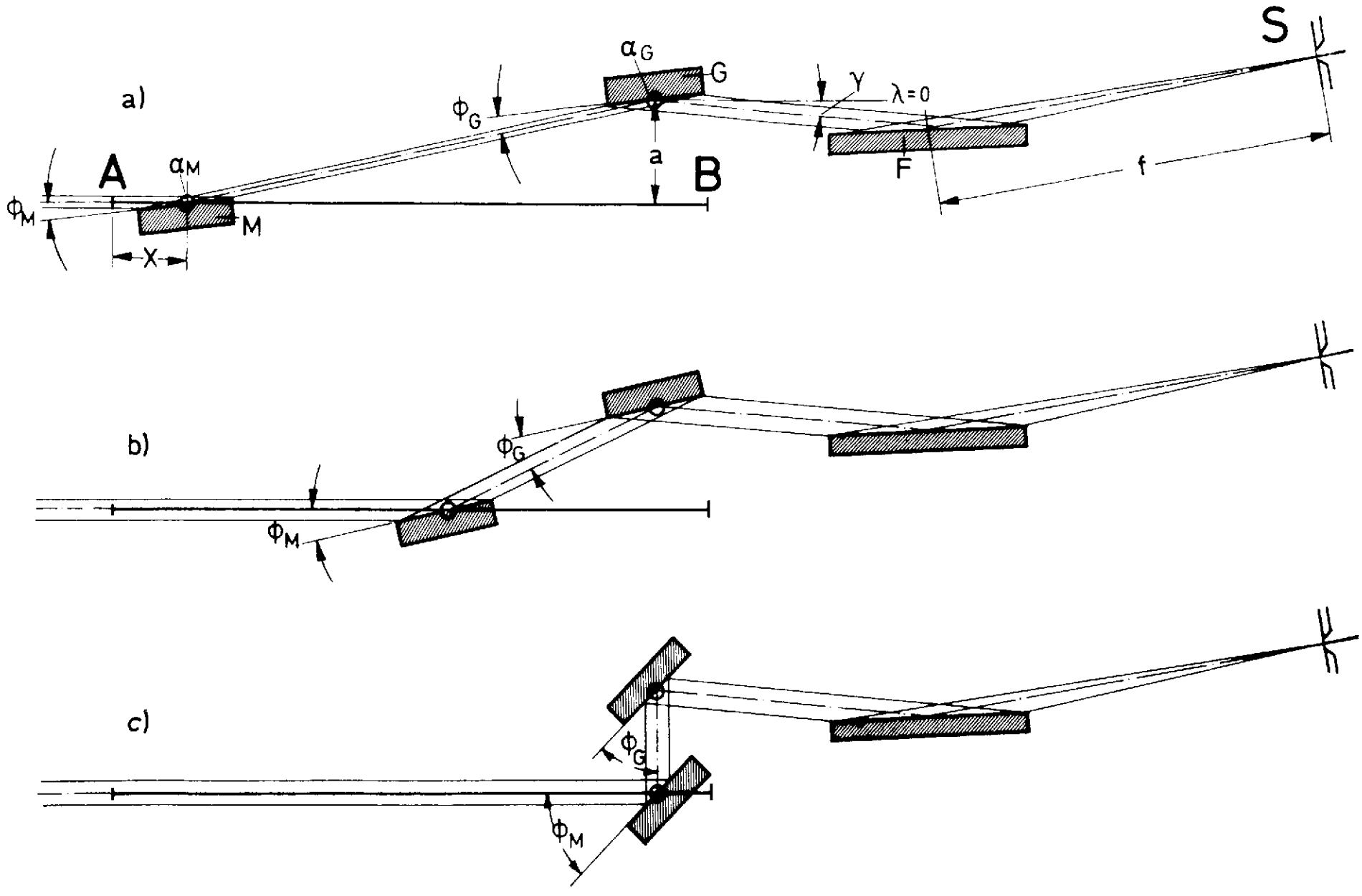
a)
A
α_M
M
X
ϕ_M
ϕ_G
α_G
G
a
B
γ
$\lambda = 0$
F
S
f
b)
ϕ_G
ϕ_M
c)
ϕ_G
ϕ_M

Fig. 1

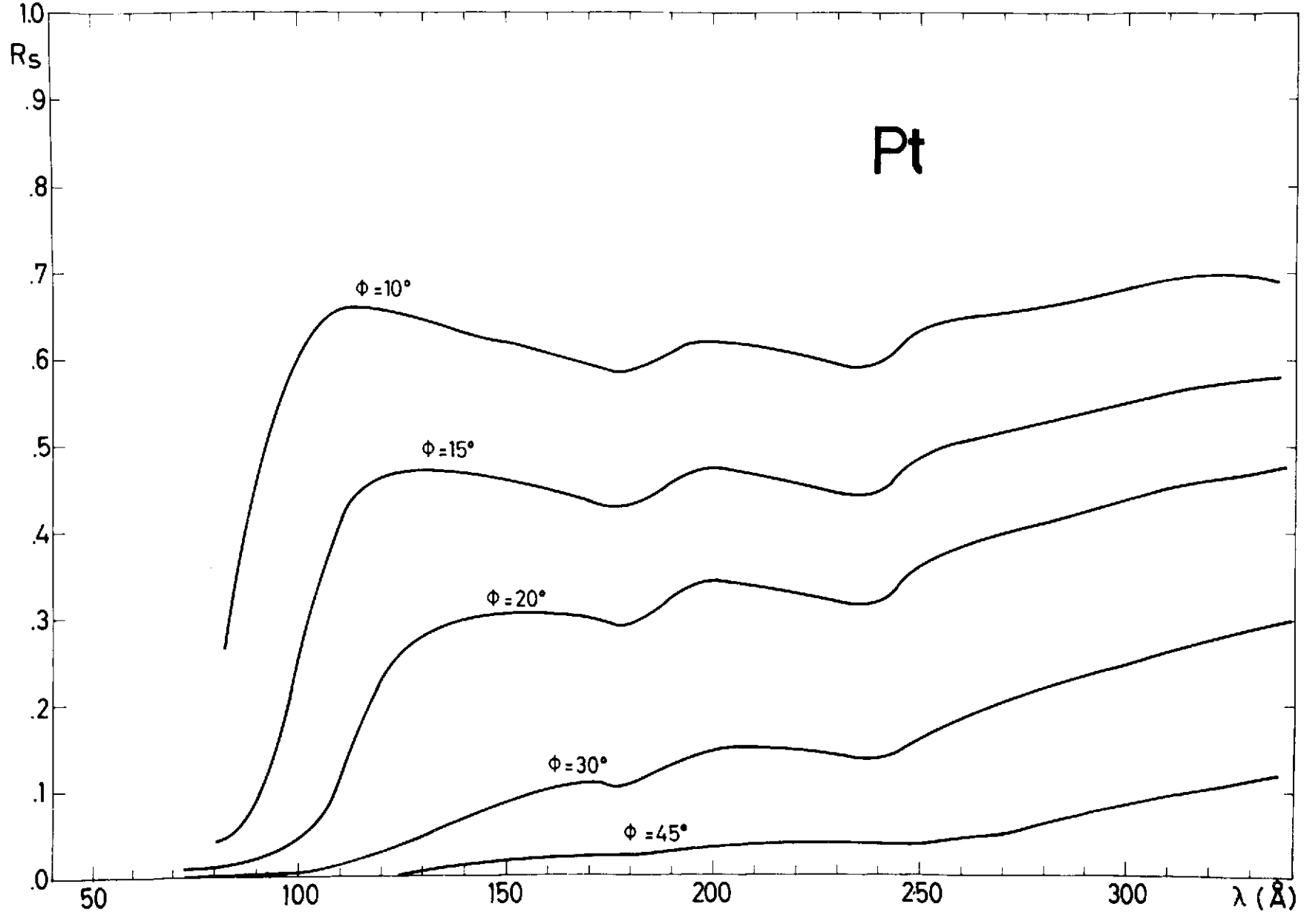
Pt
Rs
1.0
.9
.8
.7
.6
.5
.4
.3
.2
.1
.0
Φ = 10°
Φ = 15°
Φ = 20°
Φ = 30°
Φ = 45°
50
100
150
200
250
300
λ (Å)

Fig. 2

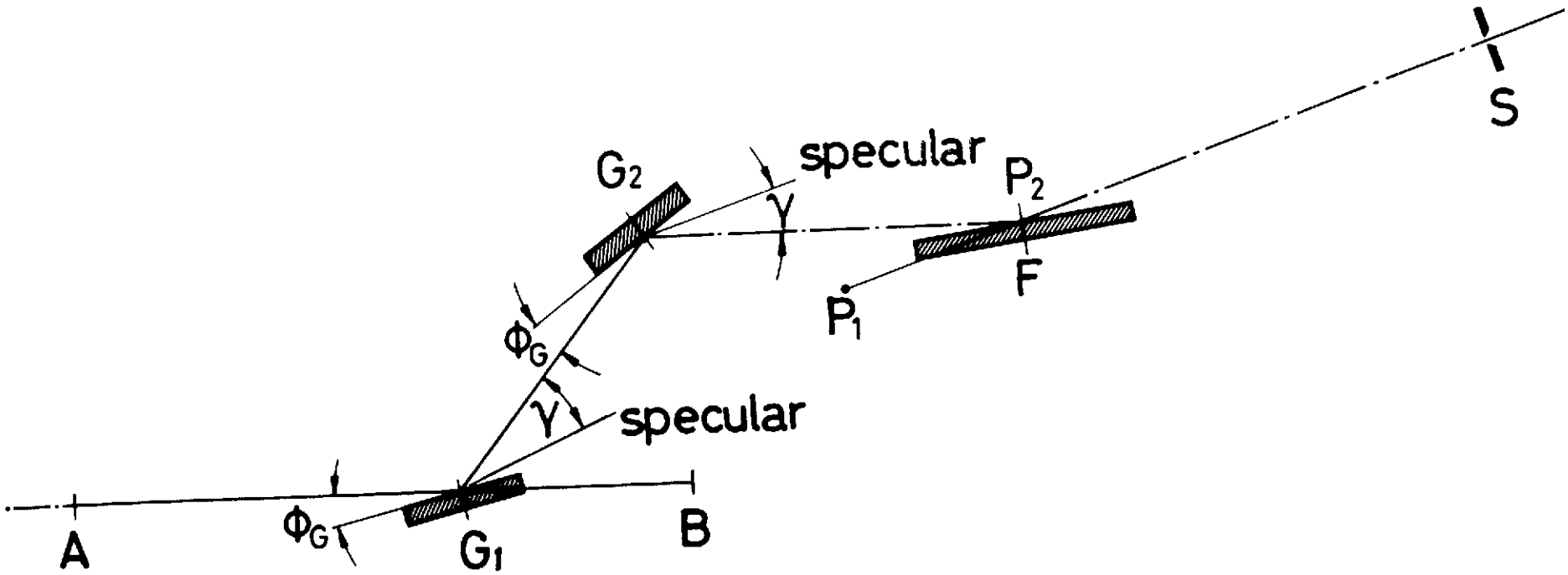

Fig. 3

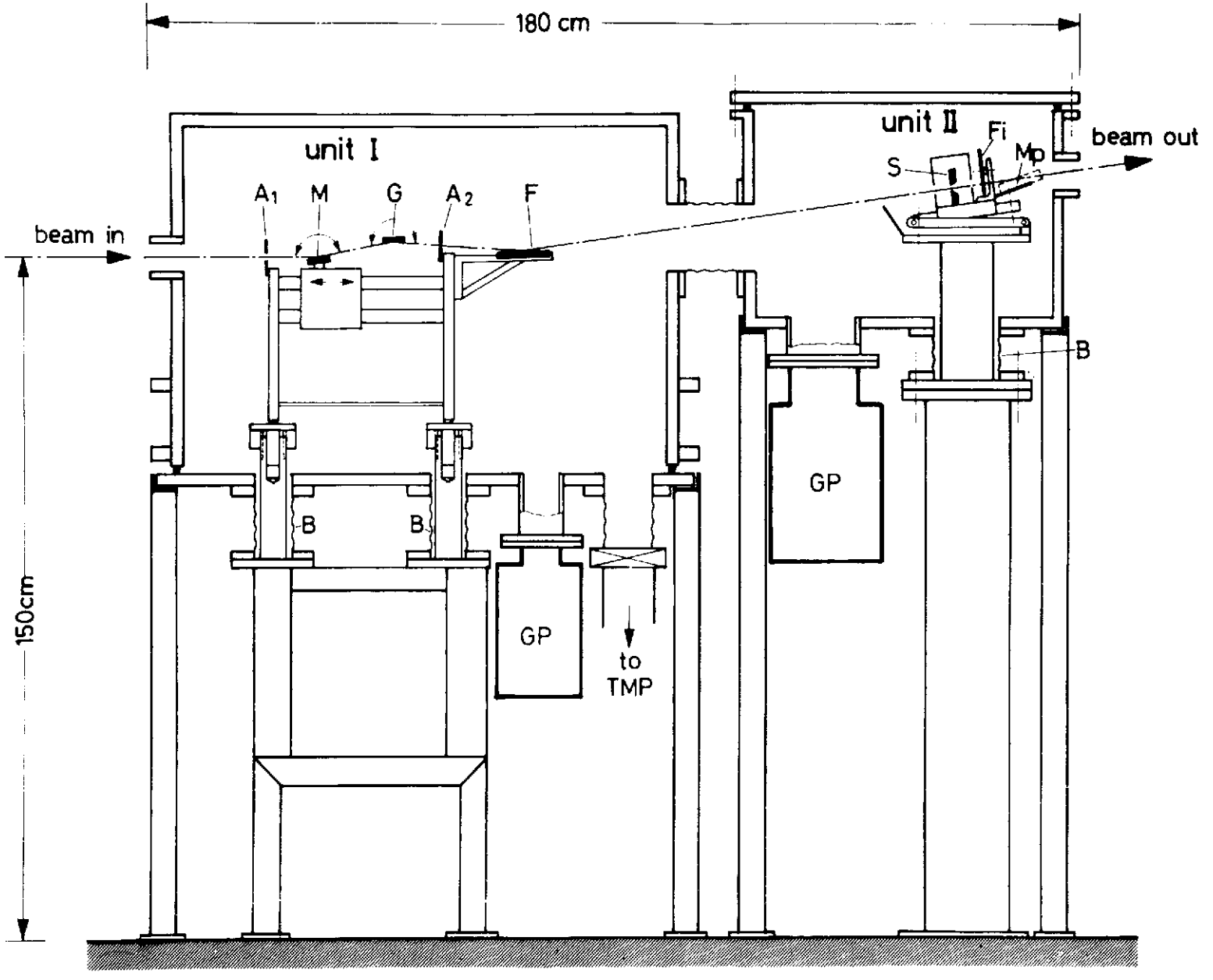
180 cm
unit I
unit II
beam in
beam out
A1
M
G
A2
F
Fi
Mp
S
B
B
B
GP
GP
to
TMP
150cm

Fig. 4

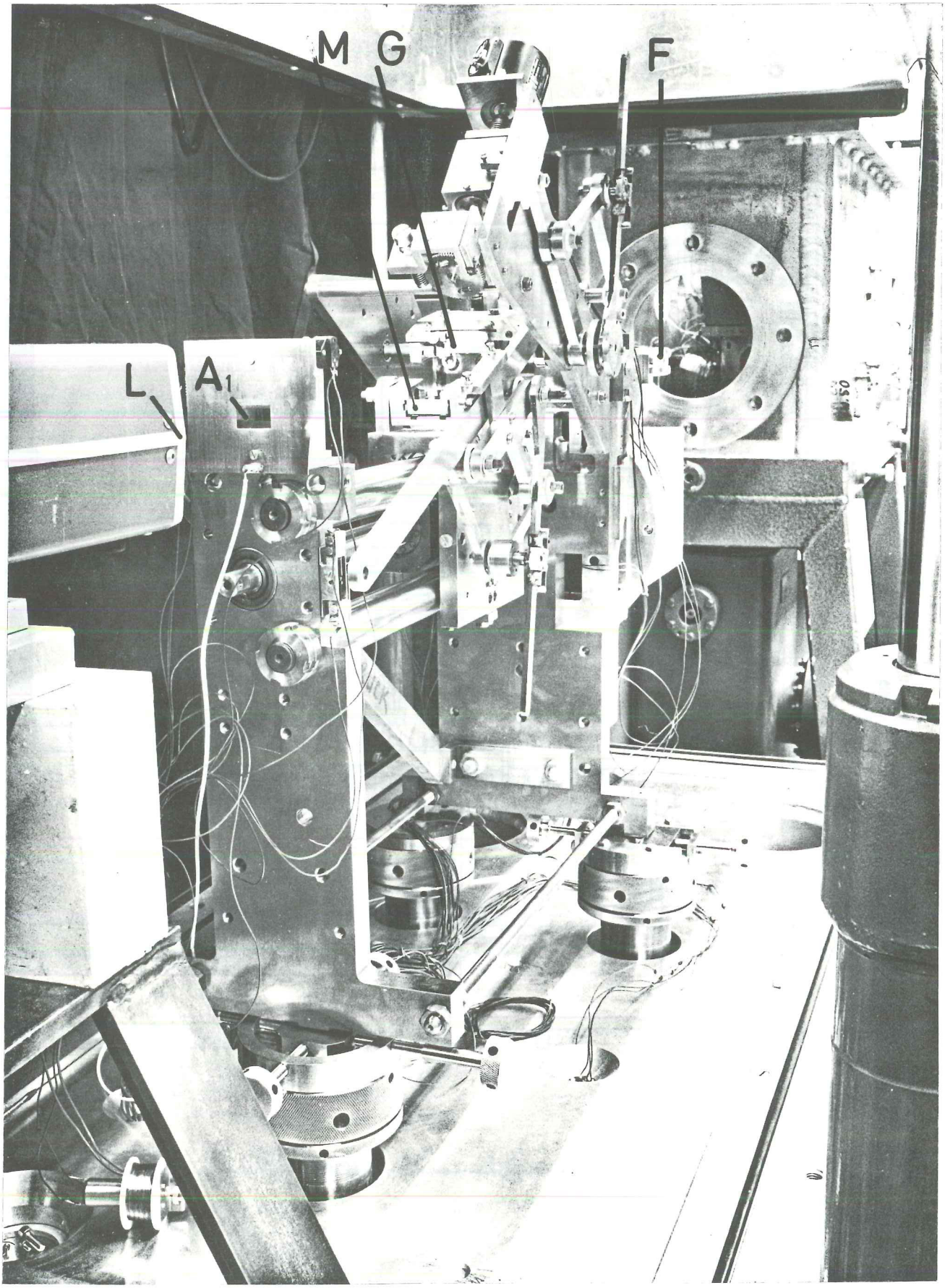

Fig. 5

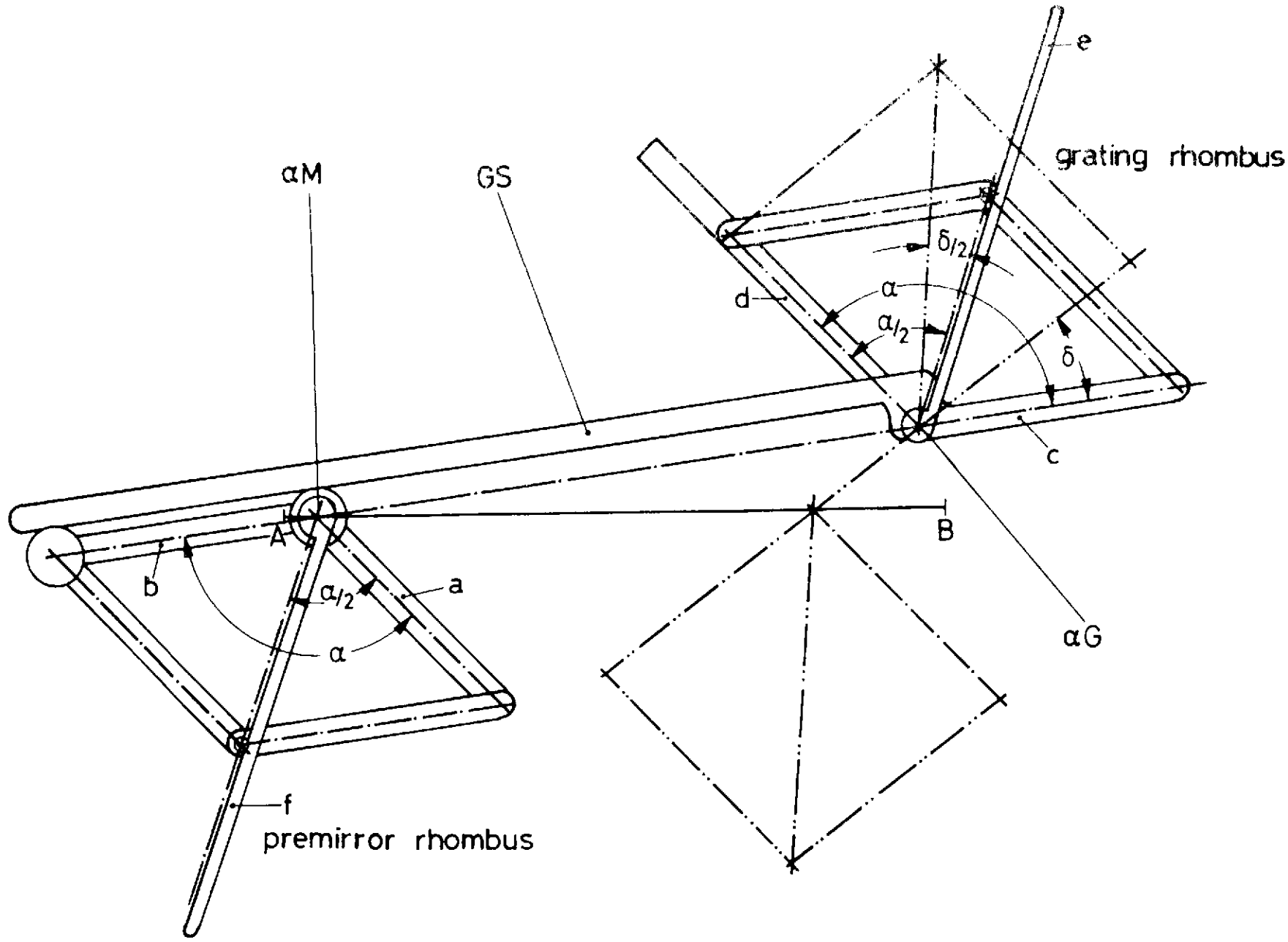
αM
GS
grating rhombus
e
δ/2
d
α
α/2
δ
c
A
B
b
a
α/2
α
αG
f
premirror rhombus

Fig. 6

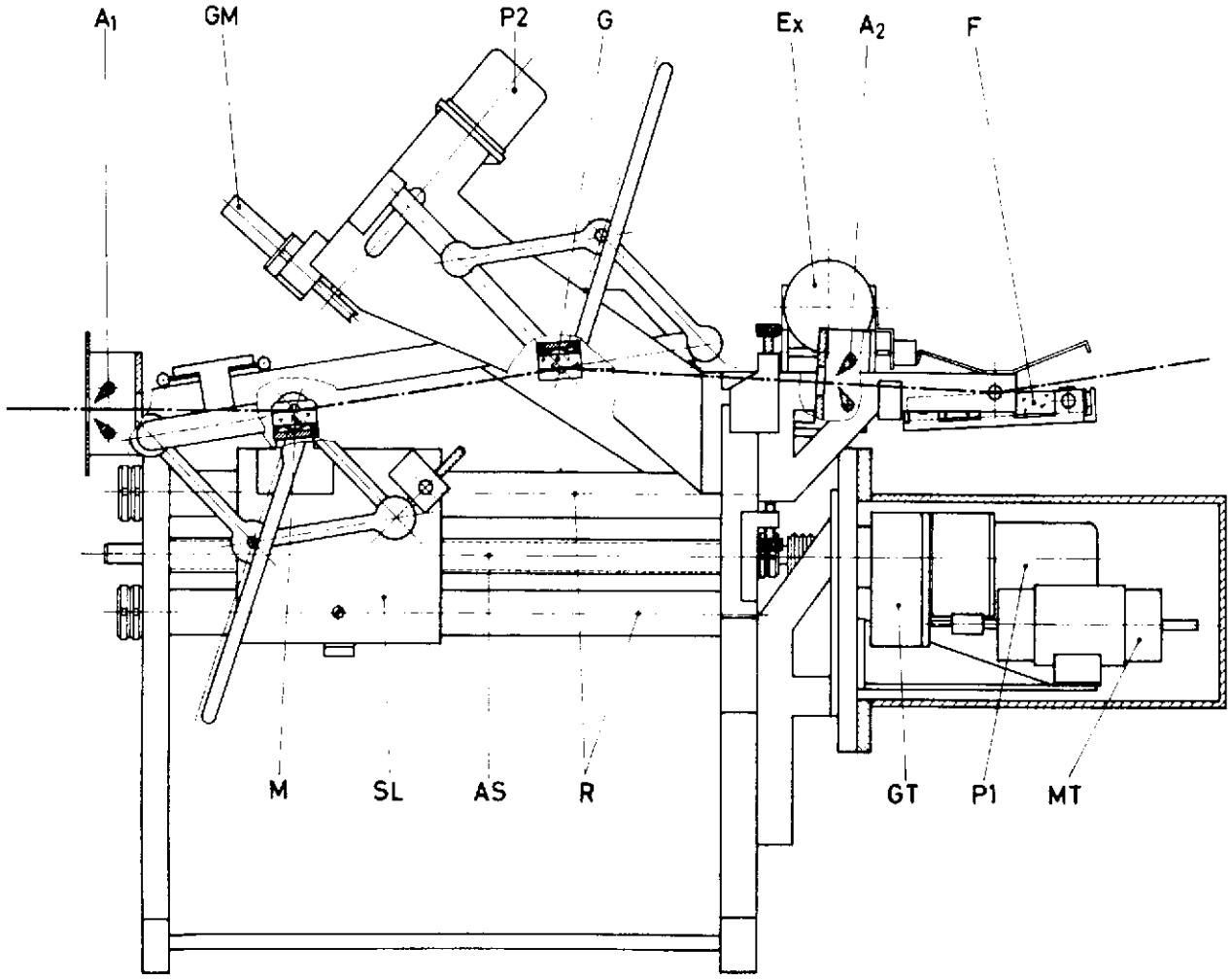

Fig. 7

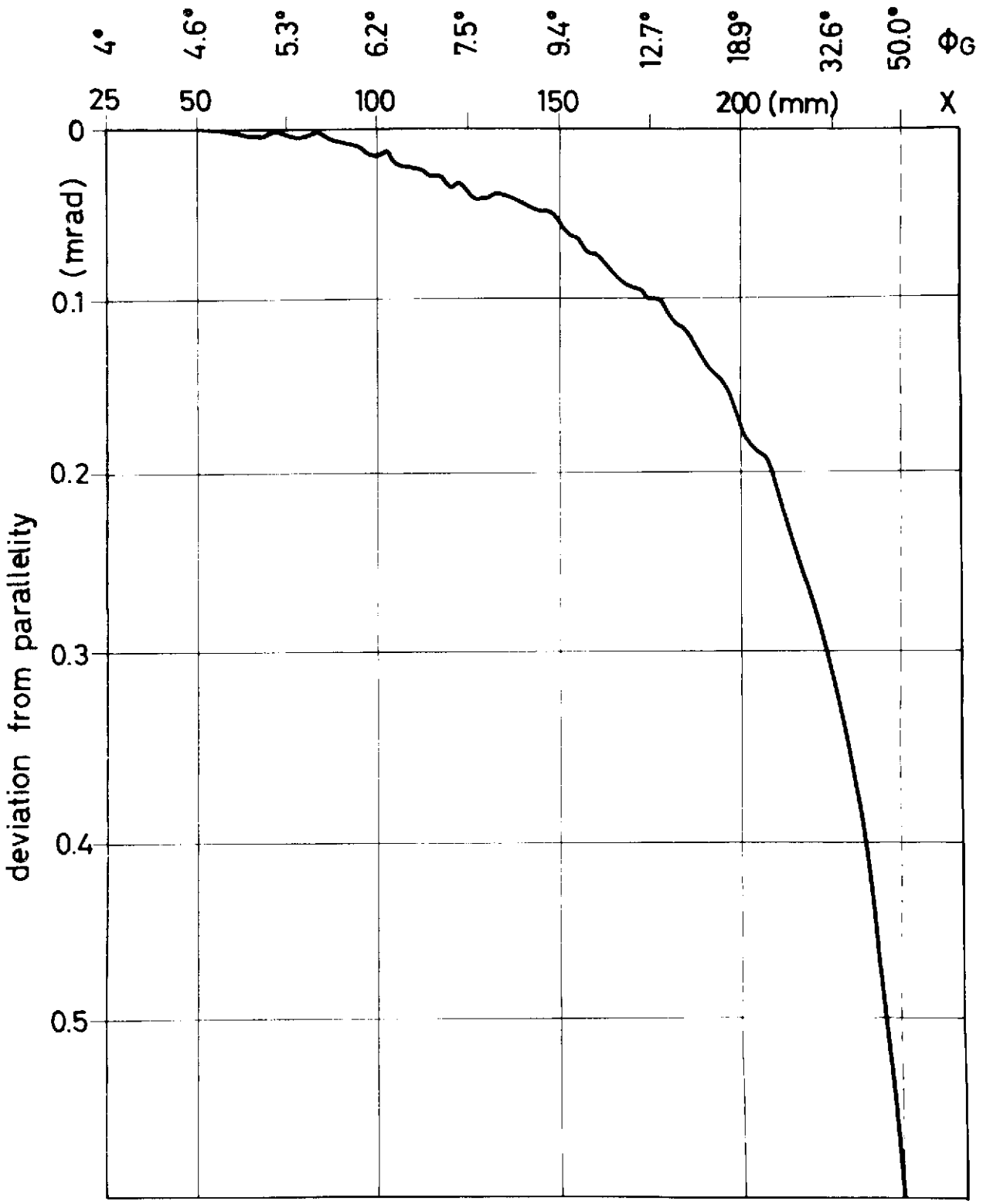
4°
4.6°
5.3°
6.2°
7.5°
9.4°
12.7°
18.9°
32.6°
50.0°
Φ_G
25
50
100
150
200 (mm)
X
0
0.1
0.2
0.3
0.4
0.5
deviation from parallelity (mrad)

Fig. 8

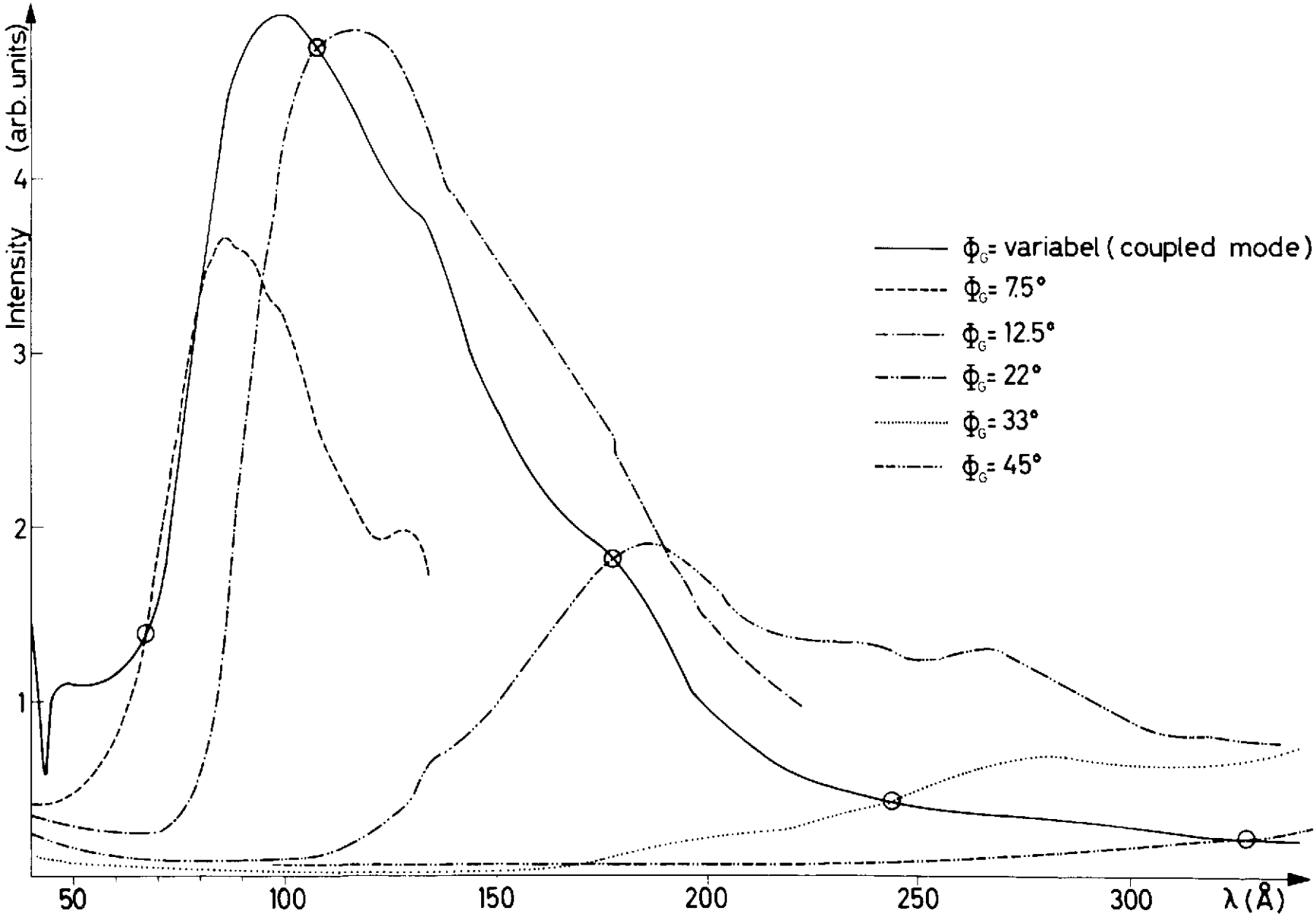
Intensity (arb. units)
1
2
3
4
50
100
150
200
250
300
λ (Å)
Φ_G= variabel (coupled mode)
Φ_G= 7.5°
Φ_G= 12.5°
Φ_G= 22°
Φ_G= 33°
Φ_G= 45°

Fig. 9

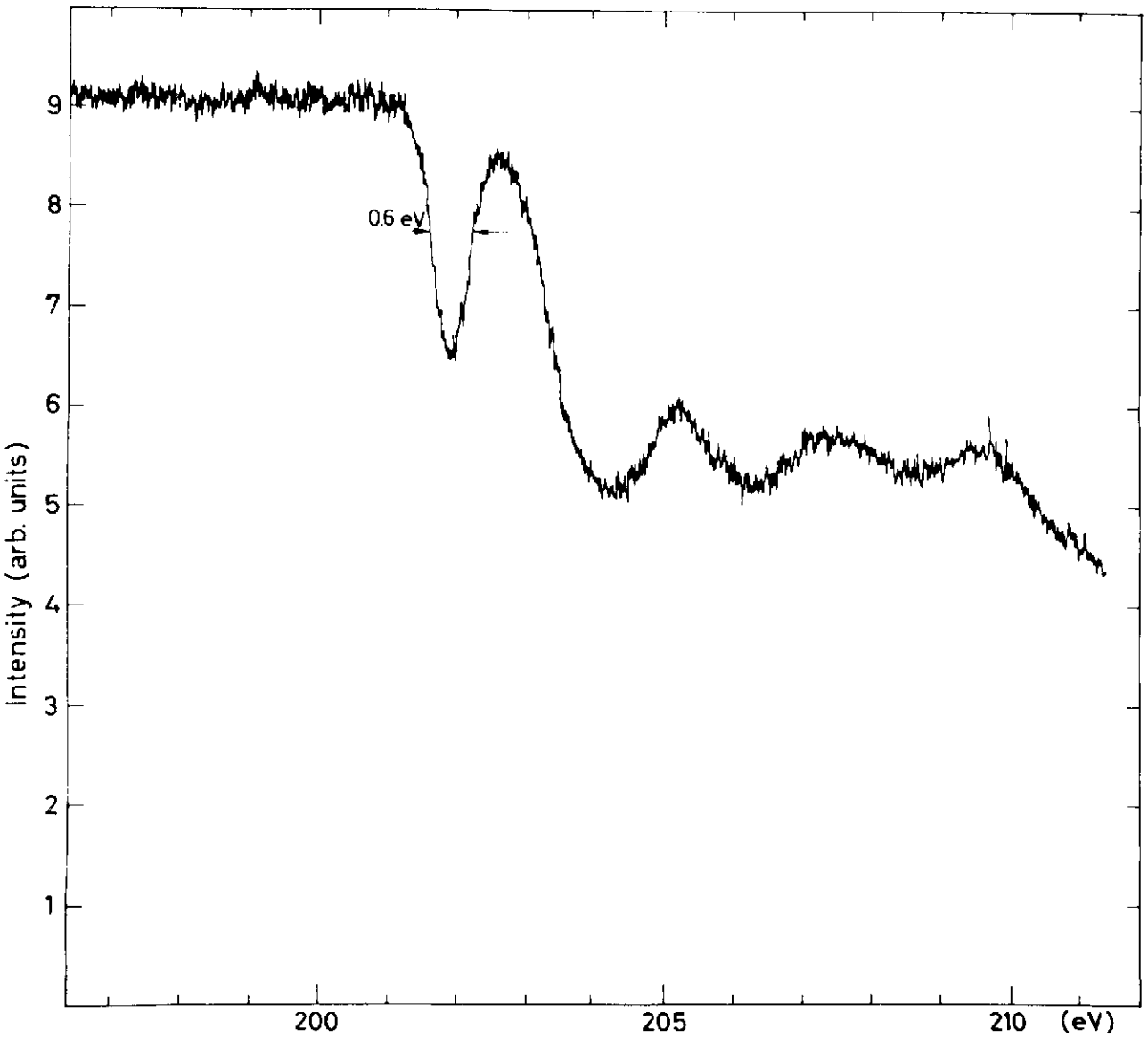

Fig. 10